Effective-medium theory of percolation on central-force elastic networks. III. The superelastic problem

E. J. Garboczi
Armstrong World Industries, Inc., Research and Development, P.O. Box 3511, 2500 Columbia Avenue, Lancaster, Pennsylvania 17604

M. F. Thorpe
Department of Physics and Astronomy, Michigan State University, East Lansing, Michigan 48824
(Received 13 September 1985)

The effective-medium theory developed in previous papers is extended to the superelastic problem, where a fraction p of the bonds in a central-force elastic network have a spring constant α_s and a fraction $1-p$ of the bonds have a spring constant α_w. The superelastic limit is obtained as $\alpha_w/\alpha_s \to 0$ such that α_w remains finite. In this paper we present comparisons between effective-medium theory and numerical simulations for the triangular net with nearest-neighbor central forces and the square net with nearest- and next-nearest-neighbor central forces. Some unexpected symmetries are found in these models.

I. INTRODUCTION

In two previous papers[1,2] we have developed an effective-medium theory for central-force networks. The theory is straightforward and can be applied to any lattice with central forces of arbitrary range. The generalization of this work to include angular forces has been difficult, but some progress has been made.[3]

In this paper we consider the application of our previous work[1,2] (henceforth referred to as I and II) to the *superelastic problem*. Consider an elastic network which has a fraction p of strong bonds α_s and a fraction $1-p$ of weak bonds α_w with $\alpha_w/\alpha_s < 1$. The limit studied in I and II corresponds to keeping α_s fixed and letting $\alpha_w \to 0$. In this paper we study the other limit in which α_w is kept fixed and $\alpha_s \to \infty$. This limit is the elastic analogue of the random mixture of superconducting and normal links and so is referred to as the *superelastic* problem. It should be emphasized that there is a single phase transition at p^* that may be approached in different ways.

In the next section we present results for the triangular net with nearest-neighbor central forces only and for a series of values of α_w/α_s that approach the superelastic limit. Comparisons are made between numerical simulations and the results of the effective-medium theory developed in I. Because of the elastic isotropy of the triangular net (that leads to $C_{11}-C_{12}=2C_{44}$) and the (unexpected) adherence to the Cauchy relation ($C_{12}=C_{44}$), even in the random system, there is effectively only one elastic constant in this system.

In Sec. III, we examine the behavior in the critical region around p^* more carefully. It is shown that the effective-medium equations give a scaling form which is reasonable except very close to p^*.

In Sec. IV we compare results of numerical simulations with effective-medium theory on the square lattice with first (α_w,α_s) and second (γ_w,γ_s) nearest-neighbor central forces. Flow diagrams for the ratio $(C_{11}+C_{12})/2C_{44}$ showing the approach to a fixed point as $p \to p^c$ reveal an interesting symmetry between the elastic and superelastic problems on this lattice.

II. TRIANGULAR NET RESULTS

We first consider the superelastic problem on a triangular net, with Hooke springs connecting nearest-neighbor sites. The potential in this case will be

$$V=\tfrac{1}{2}\sum_{\langle ij\rangle}\alpha_{ij}[(\mathbf{u}_i-\mathbf{u}_j)\cdot\hat{\mathbf{r}}_{ij}]^2 , \tag{1}$$

where the angular brackets denote a sum over nearest-neighbor pairs connected by springs with force constant α_{ij}; α_{ij} is a random variable that takes on the values α_s,α_w with probability $p,1-p$; $\hat{\mathbf{r}}_{ij}$ is a unit vector from site i to site j, and $\mathbf{u}_i$ is the displacement of site i from equilibrium. When $\alpha_w \to 0$ for α_s finite, we recover the rigidity percolation[4] problem studied in I and when $\alpha_s \to \infty$ for α_w finite we have the superelastic problem. For arbitrary values of α_s and α_w we can develop an effective-medium theory (EMT) using the *static method* derived in I.

The static method treats a single-defect spring α in an effective medium of springs with force constants α_m. This single-defect case is solved exactly, and we then average over the probability distribution for the defect springs α to get the renormalized effective force constant α_m as a function of p. The result from I is[5]

$$\left\langle \frac{\alpha_m-\alpha}{\alpha_m/a^*-\alpha_m+\alpha} \right\rangle = 0 , \tag{2}$$

where the angular brackets denote an average over the probability distribution $P(\alpha)$. Using the distribution

$$P(\alpha)=p\delta(\alpha-\alpha_s)+(1-p)\delta(\alpha-\alpha_w) , \tag{3}$$

we get the effective-medium equation

$$\frac{(\alpha_m-\alpha_s)p}{\alpha_m/a^*-\alpha_m+\alpha_s}+\frac{(\alpha_m-\alpha_w)(1-p)}{\alpha_m/a^*-\alpha_m+\alpha_w}=0\,. \tag{4}$$

Taking $\alpha_s=\alpha$, $\alpha_w\to 0$ as in I we get

$$\frac{\alpha_m}{\alpha}=\frac{p-a^*}{1-a^*}\,, \tag{5}$$

where $a^*=2d/z=\frac{2}{3}$ for the triangular net as was shown in I. Taking the superelastic limit $\alpha_s\to\infty$ we obtain

$$\frac{\alpha_w}{\alpha_m}=\frac{a^*-p}{a^*}\,. \tag{6}$$

For the triangular net with all force constants equal to α_m the elastic moduli are $C_{11}=3C_{44}=(3\sqrt{3}/4)\alpha_m$ so that Eq. (6) gives a prediction for C_{11}^{-1} and C_{44}^{-1} at all values of $p<a^*$ and predicts a phase transition at $p^*=a^*=\frac{2}{3}$ where C_{11}^{-1} and C_{44}^{-1} go to zero or equivalently the elastic moduli diverge.

We have done numerical simulations on the triangular net to check how accurate the EMT is for general values of α_s and α_w and for the superelastic limit. In I it was shown that the EMT was very accurate for the case in which $\alpha_w\to 0$. All the triangular net simulations were done on a $21\times 24=504$ atom unit cell. An external strain was imposed by redefining the vectors that define the large periodic cell. Each atom was then allowed to move toward a position of zero force. The elastic energy was then computed and the elastic moduli C_{ij} extracted via $U=\frac{1}{2}C_{ij}\epsilon^2$, where U is the elastic energy per unit volume and ϵ is the imposed strain. C_{ij} was averaged over five configurations for each value of p.

Figure 1 shows C_{11}^{-1} and C_{44}^{-1} versus p, the fraction of α_s bonds present. The units are such that $\alpha_s=10$ and $\alpha_w=1$. The solid lines were obtained from (4), which gives a quadratic equation for α_m for finite values of α_s and α_w. The agreement between EMT and simulation is almost exact. Figure 2 shows the same computation done for $\alpha_s=100$ and $\alpha_w=1$. Again EMT and simulation are in close agreement, with only some very small fluctuations around $p\simeq 0.5$–0.7. Figure 3 shows C_{11}^{-1} and C_{44}^{-1} for

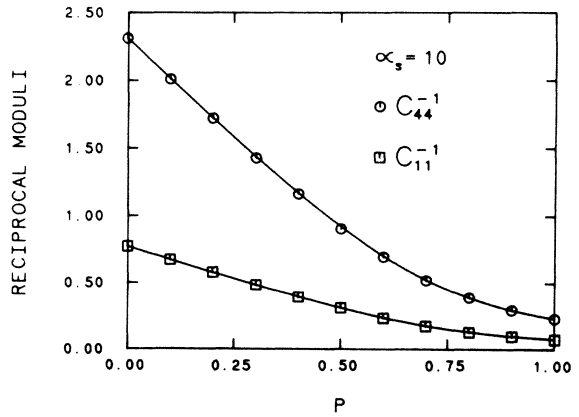

FIG. 1. Showing C_{44}^{-1}, C_{11}^{-1} vs p for the triangular net with $\alpha_s=10$, $\alpha_w=1$. The points are from simulations on a $21\times 24=504$ site network averaged over five configurations. The solid lines are the result from EMT.

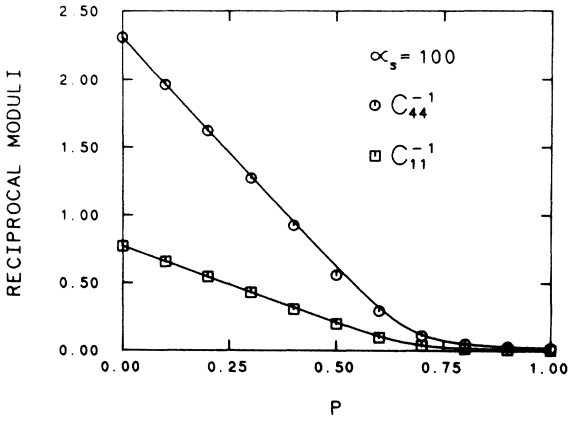

FIG. 2. Same as Fig. 1 except that $\alpha_s=100$.

$\alpha_s=10^4$ and $\alpha_w=1$. Here, the EMT is essentially a straight line because $\alpha_s/\alpha_w=10^4$ gives a result close to the limiting form in Eq. (6). The fluctuations in the reciprocal moduli are larger in this case, but within numerical error. The simulation and EMT are in excellent agreement. Near to p^* on the left-handside, some of the points seem systematically beneath the EMT line, but this could be due to relaxation difficulties. Near p^* every atom had to be moved many thousands of times in order to drive the elastic energy to its final value. An extrapolation technique was used (see II) to save computer time which gives only an upper bound on the final relaxed energy.[6] Since in Fig. 3 we are plotting the *reciprocal* moduli, reducing the energy by further relaxation would tend to bring the data points *up* and into closer agreement with the EMT. Also since α_s/α_w is so large p^* is "almost" a real critical point, near which the EMT is not necessarily accurate. And of course there are always finite size and random noise effects, particularly in the critical region, which could have made a contribution.

Figure 4 shows the ratio C_{11}/C_{44} plotted against p for the data shown in Figs. 1–3. The ratios for $\alpha_s=10,10^4$ have been rescaled to fit on one graph. The horizontal lines are the EMT result which predicts the C_{11}/C_{44} ratio will remain constant. For both $\alpha_s=10$ and 100 the nu-

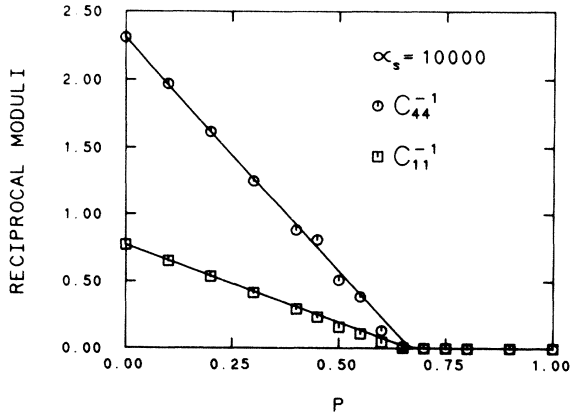

FIG. 3. Same as Fig. 2 except that $\alpha_s=10\,000$.

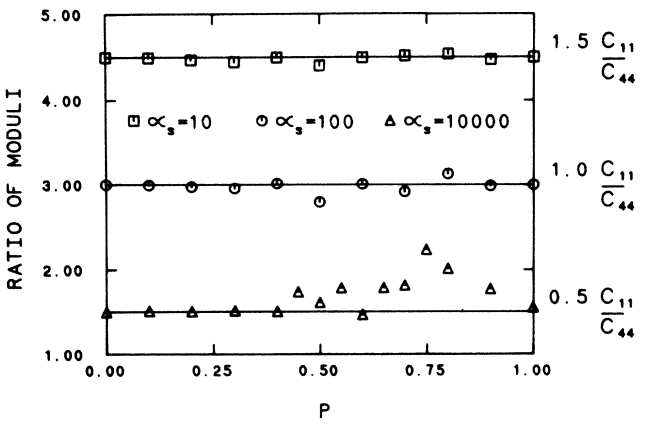

FIG. 4. Showing the C_{11}/C_{44} ratios for the data shown in Figs. 1–3. The straight lines are from EMT. Note that the factors of 0.5, 1.0, and 1.5 are introduced to offset the results.

merical simulations track the EMT rather well, with somewhat more noise than in Figs. 1 and 2 because we are dividing two computed numbers. The data for $\alpha_s=10^4$ follows the EMT line quite well until about $p=0.45$, and deviates significantly from EMT through the critical region, and then drops back to the pure system value as p approaches 1, where the system consists of all α_s bonds. The deviations of C_{11}/C_{44} from the EMT value of 3 in the critical region are at least partly due to the numerical effects discussed in Sec. II above, but could also be a real critical effect as the ratio C_{11}/C_{44} relaxes to its real critical value, which could be different from the EMT value of 3.

III. CRITICAL REGION

The EMT equation (4) can be rewritten in the critical region ($\alpha_s/\alpha_w \gg 1, |p-p^*| \ll 1$) as

$$(1-p^*)\frac{\alpha_m^2}{\alpha_s\alpha_w}-(p-p^*)\frac{\alpha_m}{(\alpha_s\alpha_w)^{1/2}}\left[\frac{\alpha_s}{\alpha_w}\right]^{1/2}-p^*=0 . \tag{7}$$

Within EMT, *all* of the elastic constants are proportional to α_m and so behave similarly. We will focus our attention on the bulk modulus $K=\frac{1}{2}(C_{11}+C_{12})$. Three limits which are of interest are discussed below.

As $\alpha_w \to 0$, but α_s remains finite, Eq. (7) becomes

$$K \sim \alpha_m = \alpha_s \frac{(p-p^*)}{(1-p^*)} \tag{8}$$

as found in I and II. More generally we would expect $K \sim (p-p^*)^f$ where the EMT in Eq. (8) gives $f=1$. Lemieux and co-workers[7] have found that $f=1.4\pm0.2$ for the central-force triangular net problem discussed in I.

As $\alpha_s \to \infty$, but α_w remains finite, Eq. (7) becomes

$$K \sim \alpha_m = \frac{\alpha_w p^*}{p^*-p} \tag{9}$$

so that the *inverse* elastic moduli go to zero linearly as p^* is approached as shown in Fig. 3. More generally we would expect $K \sim (p^*-p)^{-\bar{f}}$ where the EMT in Eq. (9) gives $\bar{f}=1$. Recently, Sahimi and Goddard[8] have found that $\bar{f}=1.12$ for the superelastic central-force problem on a triangular net.

We note in passing that Feng[9] has found that $\bar{f}=1.02\pm0.07$ and Bergman[10] has found $\bar{f}=1.30\pm0.01$ for related but different problems.

For $p=p^*$, Eq. (7) reduces to

$$K \sim \alpha_m = (\alpha_s\alpha_w)^{1/2}[p^*/(1-p^*)]^{1/2} . \tag{10}$$

In general for $p=p^*$, Eq. (4) can be rewritten as

$$\frac{\alpha_m}{(\alpha_s\alpha_w)^{1/2}} = f(\alpha_w/\alpha_s) , \tag{11}$$

where near the critical point ($\alpha_w/\alpha_s \to 0$) we would expect power-law behavior:[11]

$$f(\alpha_w/\alpha_s) \sim (\alpha_w/\alpha_s)^k , \tag{12}$$

where EMT gives $k=0$.

In Fig. 5, we show the results of numerical simulations for the bulk modulus at $p^*=\frac{2}{3}$. The effective force constant α_m can be extracted from the bulk modulus and we plot y against x where

$$x=(\alpha_w/\alpha_s)^{1/2} ,$$
$$y=\alpha_m/(\alpha_s\alpha_w)^{1/2} . \tag{13}$$

Also shown is the EMT result from Eq. (4) rewritten in the form of Eq. (11). Note that $y=1$ when $x=1$. At the critical point, we see from Eq. (10) that

$$\frac{\alpha_m}{(\alpha_s\alpha_w)^{1/2}} = \left[\frac{p^*}{1-p^*}\right]^{1/2} = \sqrt{2} \tag{14}$$

so that $y=\sqrt{2}$ when x is very small. The EMT agrees well with the simulation results down to $\log_{10}x \simeq -1.0$, which corresponds to $\alpha_s \simeq 100\alpha_w$. For smaller values of x, there are significant differences. Note that the simulation results have large error bars in this region because of

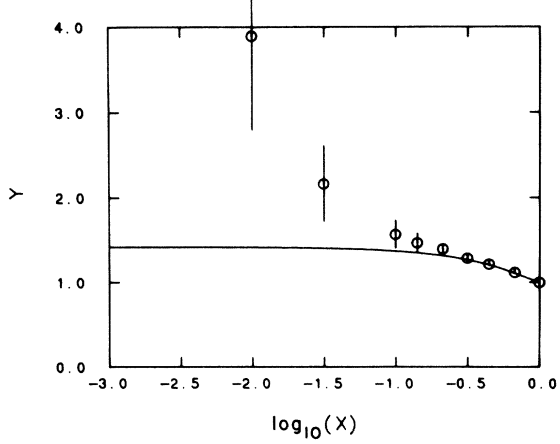

FIG. 5. Results of simulations and EMT are shown at $p=p^*=\frac{2}{3}$. The variables are $y=\alpha_m/(\alpha_s\alpha_w)^{1/2}$ and $x=(\alpha_w/\alpha_s)^{1/2}$. The EMT result (see Sec. III) can be written as $y=\frac{1}{2}[(8+x^4)^{1/2}-x^2]$ so that $y=1$ when $x=1$ and $y=\sqrt{2}$ when $x=0$.

increasing fluctuations between configurations as the superelastic limit is approached. Also the simulations were carried out at $p^*=\frac{2}{3}$ (as a test of EMT) rather than at the best current numerical estimate for the critical point, which is $p^*=0.649$.[7,8]

IV. SQUARE NET RESULTS

Another system on which we have studied the superelastic problem is the square net with first- and second-nearest-neighbor Hooke springs. The potential is given by

$$V=\tfrac{1}{2}\sum_{i,j}[(\mathbf{u}_i-\mathbf{u}_j)\cdot\hat{\mathbf{r}}_{ij}]^2\alpha_{ij} + \tfrac{1}{2}\sum_{i,j}[(\mathbf{u}_i-\mathbf{u}_j)\cdot\hat{\mathbf{r}}'_{ij}]^2\gamma_{ij}\ , \tag{15}$$

where the first sum is over all nearest-neighbor bonds and the second is over all second-nearest-neighbor bonds. α_{ij} (γ_{ij}) is a random variable which takes on the values α_s,α_w (γ_s,γ_w) with probabilities p_1, $1-p_1$ (p_2, $1-p_2$), and $\hat{\mathbf{r}}_{ij}$ and $\hat{\mathbf{r}}'_{ij}$ are unit vectors between first- and second-neighbor pairs of sites, respectively. When $p_1=p_2=0$ and all of the springs are α_w or γ_w, then the elastic moduli are given by

$$C_{11}=\alpha_w+\gamma_w\ ,\quad C_{44}=C_{12}=\gamma_w\ ,\quad K=\tfrac{1}{2}\alpha_w+\gamma_w\ , \tag{16}$$

where $K=\frac{1}{2}(C_{11}+C_{12})$ is the bulk modulus.

An EMT can easily be derived for the square net with potential (15) in complete analogy with that developed in II and in Sec. II of this paper. Using these methods we get two EMT equations, one for the α bonds and one for the γ bonds:

$$\frac{(\alpha_m-\alpha_s)p_1}{\alpha_m/a_1^*-\alpha_m+\alpha_s}+\frac{(\alpha_m-\alpha_w)(1-p_1)}{\alpha_m/a_1^*-\alpha_m+\alpha_w}=0\ , \tag{17}$$

$$\frac{(\gamma_m-\gamma_s)p_2}{\gamma_m/a_2^*-\gamma_m+\gamma_s}+\frac{(\gamma_m-\gamma_w)(1-p_2)}{\gamma_m/a_2^*-\gamma_m+\gamma_w}=0\ , \tag{18}$$

where $a_1^*+a_2^*=1$ is an identity and a_1^* is given by

$$a_1^*=\frac{1}{\pi^2}\int_0^\pi\int_0^\pi dK_x dK_y\,\frac{2(1-r_m)-(2+r_m)(C_x+C_y)+(2+r_mC_x+r_mC_y)C_xC_y}{1+2r_m+r_m^2(C_x-C_y)^2+(1-2r_m)C_xC_y-(1+r_m-r_mC_xC_y)(C_x+C_y)}\ , \tag{19}$$

and $r_m=\gamma_m/\alpha_m$, $C_x=\cos(K_xa)$, $C_y=\cos(K_ya)$, and a is the nearest-neighbor distance on the square net. The dependence of a_1^* on the ratio γ_m/α_m couples the two EMT equations.

Taking the limits $\alpha_w,\gamma_w\to 0$ with α_s,γ_s finite reduces Eqs. (17) and (18) to

$$\frac{\gamma_m}{\gamma_s}=\frac{p_2-a_2^*}{1-a_2^*}\ , \tag{20}$$

$$\frac{\alpha_m}{\alpha_s}=\frac{p_1-a_1^*}{1-a_1^*}\ , \tag{21}$$

which was the form of the EMT equations used in II for the ordinary elastic problem. The superelastic limit is obtained when $\alpha_s,\gamma_s\to\infty$ with α_w,γ_w finite, resulting in the EMT equations

$$\frac{\gamma_w}{\gamma_m}=\frac{a_2^*-p_2}{a_2^*}\ , \tag{22}$$

$$\frac{\alpha_w}{\alpha_m}=\frac{a_1^*-p_1}{\alpha_1^*}\ . \tag{23}$$

Equations (22) and (23) imply that the superelastic phase transition occurs when $p_1^c=a_1^*$ and $p_2^c=a_2^*$ or, since $a_1^*+a_2^*=1$, the transition occurs along the line $p_1^c+p_2^c=1$ in the p_1,p_2 phase plane.

Figure 6 shows the p_1,p_2 phase plane for the square net. The large-dashed line is the critical line $p_1^c+p_2^c=1$. The upper right-hand region of Fig. 6 has $\alpha_w,\gamma_w\to 0$ with α_s,γ_s finite. Tracks 1 and 2 start from $p_1=p_2=1$ and finish on the critical line where all of the elastic moduli go to zero for the elastic problem analyzed in II. The lower left-hand region of Fig. 6 has $\alpha_s,\gamma_s\to\infty$ with α_w,γ_w finite. Tracks 3 and 4 start at $p_1=p_2=0$ and finish on the critical line where all of the elastic moduli diverge.

Numerical simulations were done for the system defined above to determine how well the EMT would describe the superelastic problem on the square net and, in particular, what the critical elastic modulus ratios would be for this problem. The details of the simulations were the same as those described in II. We have computed

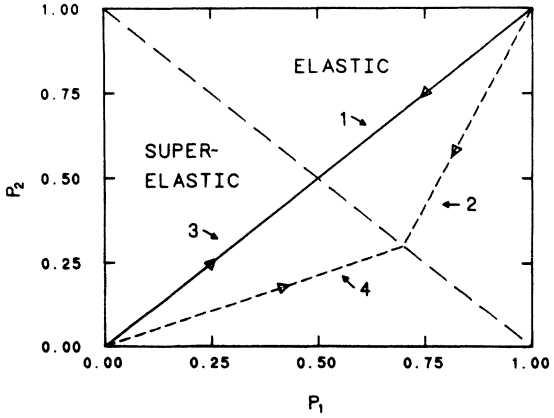

FIG. 6. Showing the p_1,p_2 phase plane for the square net with first- and second-nearest-neighbor springs. The side labeled "elastic" has $\alpha_w,\gamma_w\to 0$ with α_s,γ_s finite while the side labeled "superelastic" has $\alpha_s,\gamma_s\to\infty$ with α_w,γ_w finite. Tracks 1–4 are defined in Sec. IV.

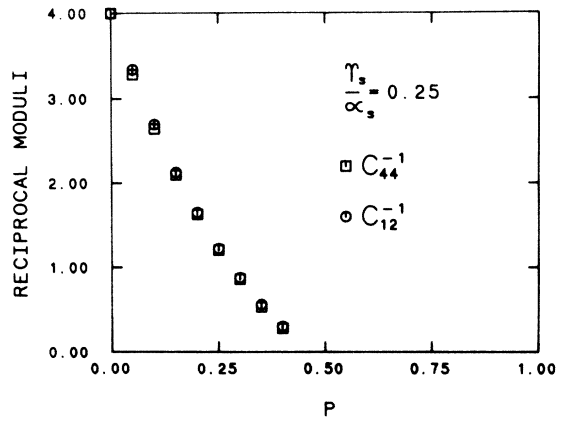

FIG. 7. Showing C_{12} and C_{44} computed along track 3 for $\gamma_s/\alpha_s=0.25$.

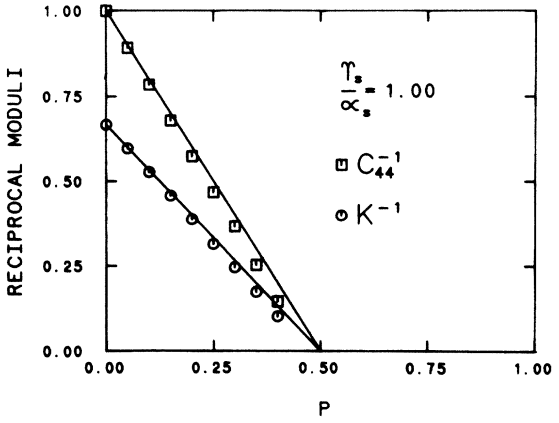

FIG. 9. Same as Fig. 8 except that $\gamma_s/\alpha_s=1.0$.

K^{-1} and C_{44}^{-1} along track 3 shown in Fig. 6, which has $p_1=p_2$, for various ratios of $\gamma_w/\alpha_w=\gamma_s/\alpha_s$.

In Fig. 7 we show the results for C_{12} and C_{44} when $\gamma_w/\alpha_w=\gamma_s/\alpha_s=0.25$, and $\gamma_s/\gamma_w=\alpha_s/\alpha_w=10^4$. It appears that, within the numerical scatter, $C_{12}=C_{44}$ for the values of $p=\frac{1}{2}(p_1+p_2)$ shown. From Eq. (16) we see that $C_{12}=C_{44}$ holds for the pure system. This is because the square net with only one kind of first- and one kind of second-nearest-neighbor force constants obeys Cauchy's theorem[12], whose proof demands that all forces must be central and each site must be at center of symmetry. It is as yet unclear why Cauchy's theorem appears to be still obeyed for these random systems. We will assume that Cauchy's theorem holds over the entire p_1,p_2 phase plane shown in Fig. 6.

Figures 8–10 show the results for K^{-1} and C_{44}^{-1} compared with the solid lines, which are the EMT result. Again there is good agreement between simulation and EMT. The only significant errors appear near $p^c=0.5$, where the data points are generally somewhat below the EMT curve. There were difficulties relaxing the systems in this region, so that our computed moduli are slightly higher than if complete relaxation of the elastic energy had been achieved. Since we are plotting the reciprocals of the moduli, complete relaxation would tend to bring the simulations and the EMT into closer agreement. Notice that the EMT results have significant curvature because of the coupling between the equations for α_m and γ_m.

Figure 11 shows the flow diagram for the ratio K/C_{44} for *both* the superelastic and elastic problems. On the left-hand side are the data for the superelastic problem computed along track 3 and on the right-hand side are the data for the elastic problem[13] computed along track 1. Both sets of data appear to be flowing towards the EMT fixed point of $K/C_{44}=1.5$, which corresponds to $\gamma_m/\alpha_m=1$. The EMT ratio curves for the elastic and superelastic cases are just reflections of each other about the point $p^c=0.5$. This is a curious symmetry, and will be proven below.

The EMT ratio equations are the following: For the elastic case,

$$r_m=\frac{\gamma_m}{\alpha_m}=\frac{r_s(p_2-a_2^*)(1-a_1^*)}{(p_1-a_1^*)(1-a_2^*)}\ , \tag{24}$$

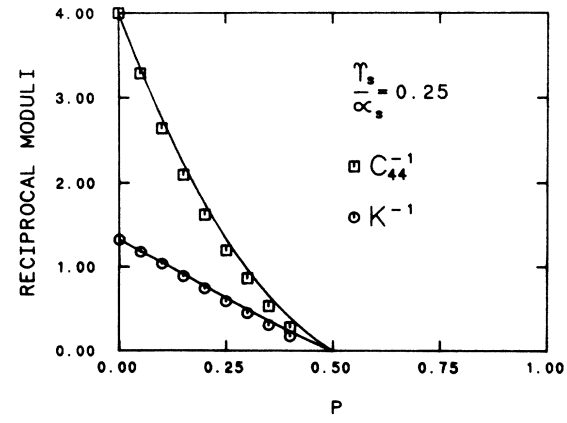

FIG. 8. Showing C_{44}^{-1} and K^{-1} vs $p=\frac{1}{2}(p_1+p_2)$ computed along track 3 for the square net with $\gamma_s/\alpha_s=0.25$, $\alpha_s/\alpha_w=\gamma_s/\gamma_w=10^4$.

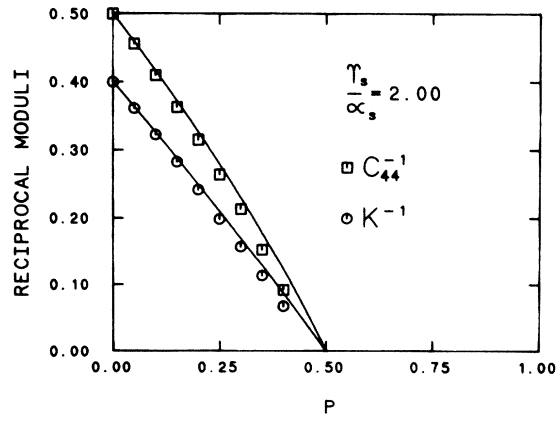

FIG. 10. Same as Fig. 9 except that $\gamma_s/\alpha_s=2.0$.

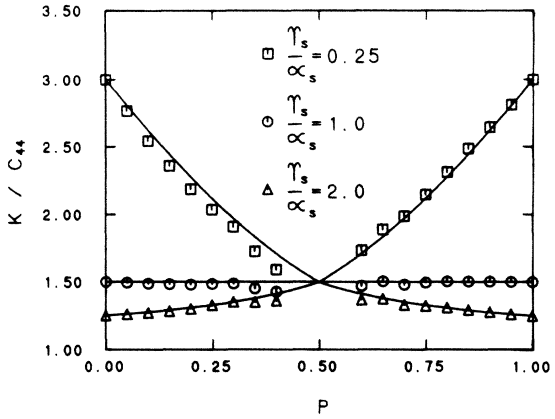

FIG. 11. Flow diagram along track 1 (elastic case, $p>0.5$) and track 3 (superelastic case, $p<0.5$) showing that K/C_{44} becomes independent of the initial value of $\gamma_w/\alpha_w=\gamma_s/\alpha_s$ at the critical point $p^c=0.5$. The solid lines are from EMT and the points are from the simulations shown in Figs. 8–10. The EMT lines shown are symmetric about $p^c=0.5$.

while for the superelastic case,

$$r_m=\frac{\gamma_m}{\alpha_m}=\frac{r_w(a_1^*-p_1)a_2^*}{(a_2^*-p_2)a_1^*}\ , \tag{25}$$

where $r_s=\gamma_s/\alpha_s=\gamma_w/\alpha_w=r_w$. Consider a general track in the p_1,p_2 phase plane like track 2 shown in Fig. 6. The equation of this line is

$$p_2=mp_1+1-m\ , \tag{26}$$

where m is the slope. This track crosses the critical line at $(m/1+m,1/1+m)$. Now make the transformation $p_1\to 1-p_2,p_2\to 1-p_1$. Equation (26) becomes

$$p_2=p_1/m \tag{26'}$$

which is the equation of the line shown as track 4, which also crosses the critical line at the same point as track 2. Now make the same transformation of variables in the superelastic ratio equation (25). It is easy to see that it then becomes identical with the *elastic* ratio equation (24). We therefore have the result that K/C_{44} versus p for the superelastic case computed along track 4 is the same, under EMT, as K/C_{44} versus p for the elastic case plotted along track 2. Figure 11 has the results for tracks 1 and 3, which have $m=m^{-1}=1$. We do not know whether this symmetry is exact or just correct within the EMT framework.

V. CONCLUSIONS

We have shown that effective-medium theory gives an excellent description of a wide variety of central-force problems, including those in the superelastic limit. The only exceptions are very close to the critical point p^* where the EMT predictions appear not to be correct although are very close. For example, for the triangular net, $p^*=0.65$ rather than $\frac{2}{3}$ and $f=1.4$, $\bar{f}=1.12$ rather than $f=\bar{f}=1$.

Similar results are obtained for the square net although accurate numerical calculations for p^* and $f,\bar{f}$ are not currently available.

All of the results of this paper and of the previous two show that the Cauchy relation ($C_{12}=C_{44}$) is obeyed with remarkable numerical accuracy for these random central-force systems. This result is of course built into the EMT equations which map the random systems on to the best nonrandom system. This nonrandom system satisfies the conditions for Cauchy's relation as usually stated.[12]

The square net exhibited an unusual symmetry that maps the flow diagram for K/C_{44} in the elastic region on to the superelastic region. This symmetry has been shown explicitly for the EMT equations and also appears from the numerical results to be exactly obeyed. It is presumably associated with a rotation of the lattice by 45° which interchanges the α and γ bonds, but we have been unable to uncover its precise nature explicitly.

ACKNOWLEDGMENTS

We thank D. A. Bruce for useful discussions. The financial support of one of us (M.F.T.) by the National Science Foundation under Grant No. DMR-83-17610 is gratefully acknowledged.

[1]S. Feng, M. F. Thorpe, and E. J. Garboczi, Phys. Rev. B **31**, 276 (1985).
[2]E. J. Garboczi and M. F. Thorpe, Phys. Rev. B **31**, 7276 (1985).
[3]L. M. Schwartz, S. Feng, M. F. Thorpe, and P. N. Sen, Phys. Rev. B **32**, 4607 (1985).
[4]M. F. Thorpe, J. Non-Cryst. Solids **57**, 355 (1983).
[5]There is a misprint in Ref. 1. In Eq. (8) α^* should be a^*.
[6]E. J. Garboczi, Ph.D. thesis, Department of Physics and Astronomy, Michigan State University, 1985.
[7]M. A. Lemieux, P. Breton, and A.-M. S. Tremblay, J. Phys. (Paris) Lett. **46**, L1 (1985).
[8]M. Sahimi and J. D. Goddard, Phys. Rev. B **32**, 1869 (1985).
[9]S. Feng, Phys. Rev. B **32**, 5793 (1985).
[10]David J. Bergman, Phys. Rev. B **33**, 396 (1986).
[11]See, for example, H. E. Stanley, *Introduction to Phase Transitions and Critical Phenomena* (Oxford University, New York, 1971).
[12]A. E. H. Love, *A Treatise on the Mathematical Theory of Elasticity*, 4th ed. (Cambridge University Press, Cambridge, England, 1934); M. Born and K. Huang, *Dynamical Theory of Crystal Lattices* (Clarendon, Oxford, 1966).
[13]The data for the elastic side of Fig. 11 are taken from Ref. 2. We computed C_{11}, C_{44}, and K in that work, but presented C_{11}, C_{44}, and $C_{12}=2K-C_{11}$.